

Dynamic Instability and Time Domain Response of a Model Halide Perovskite Memristor for Artificial Neurons

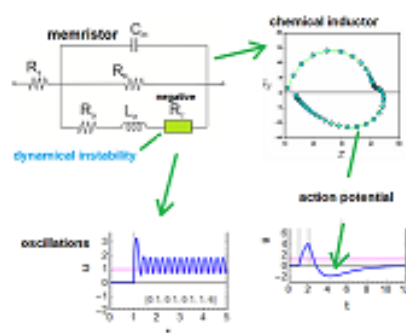
Juan Bisquert,*¹ Antonio Guerrero¹

¹Institute of Advanced Materials (INAM), Universitat Jaume I, 12006 Castelló, Spain.

Corresponding author J. Bisquert (bisquert@uji.es)

Abstract

Memristors are candidate devices to construct artificial neurons, synapses and computational networks for brain-like information processing and sensory-motor autonomous systems. However, the dynamics of natural neurons and synapses are challenging and cannot be well reproduced with standard electronic components. Halide perovskite memristors operate by mixed ionic-electronic properties that may lead to replicate the live computation elements. Here we explore the dynamical behaviour of a halide perovskite memristor model to evaluate the response to a step perturbation and the self-sustained oscillations that produce analog neuron spiking. As the system contains a capacitor and a voltage-dependent chemical inductor, it can mimic an action potential in response to a square current pulse. Furthermore, we discover a property that cannot occur in the standard two-dimensional model systems: a three-dimensional model shows a dynamical instability that produces a spiking regime without the need for an intrinsic negative resistance. These results open a new pathway to create spiking neurons without the support of electronic circuits.



The processing of information and sensory data managing in networks of neurons and synapses in the brain occurs by stimulation of neurons causing repeated action potentials in periodic rhythms.¹⁻³ To construct artificial brain-like computation and sensory-motor autonomous systems, we need networks of miniature elements that perform and distribute rhythmic spiking.⁴⁻⁷ Currently many CMOS-based neuromorphic computation systems use very simple integrate and fire neurons.⁸ These consist basically of a RC (resistance-capacitor) circuit that becomes progressively charged and discharges suddenly when the voltage exceeds a threshold value.

However, natural spikes have more complex properties like a refractory post-spike period.⁹ The natural neuron spiking is a self-sustained oscillation connected to dynamical instability.³ A Hopf bifurcation is a critical point where the system destabilizes and a periodic behavior that never reaches equilibrium arises.^{10,11} The spiking patterns are well described by dynamical models formed by a few differential equations, based on the pioneering work of Hodgkin and Huxley on the giant axon of the squid.² Many useful simplified models with a lower number of equations as the FitzHugh-Nagumo model have been derived¹¹⁻¹⁵ and classified by the number and type of equations and the dynamic and bifurcation properties.¹¹ We have recently described the conditions for Hopf bifurcation and spiking regimes in two-dimensional models, using the methods of equivalent circuits (EC) and impedance spectroscopy.¹⁶ We concluded that the main elements needed for a self-sustained oscillation to occur are: (1) a membrane capacitor, (2) a chemical inductor, (3) a built-in negative resistance.¹⁷

A memristor is a two-terminal device whose resistance depends on the history of current and voltage applied to the device. Memristors allow the storage of information by metastable modification of device conductivity.¹⁸⁻²² Memristor devices are the main candidates to produce compact and reliable artificial neurons and synapses for computation algorithms based on neuron spiking.^{9,18,19,22-27} Recently halide perovskite memristors have been investigated, as their ionic-electronic properties and strong hysteresis effects are promising for neuromorphic applications.^{18,19,28-30} Halide perovskites produce synapse-like functionality with a simple structure and extremely low energy consumption.^{26,31} The question is, can we generate the analog neuron properties of spiking neurons with memristors? This property requires the presence of instabilities in addition to the memory conductance effects.

To address this topic, we use here a model for a halide perovskite memristor that has recently been shown to describe well the experimental current-voltage cycling and impedance response.³² This type of model may be applied with suitable adaptations to a variety of material platforms such as mixed ionic-electronic organic materials.^{5,9,33} Here we analyze the time transient voltage response to step stimulation, the stability, and the bifurcation properties of this model using the EC methods.^{16,17}

The model will be presented in different steps. We first describe a two-dimensional simplified version of the model that enables to calculate the transient response to a voltage or current pulse as it is usually done for the analysis of synapsis potentiation and

plasticity.^{26,30,34,35} Then we present the three-dimensional model and we show that it presents a dynamical instability in which self-sustained oscillations occur without the need for an intrinsic negative resistance, in contrast to the two-dimensional models.

The two-dimensional model

We discuss the dynamical memristor model formed by the system of equations³²

$$I_{tot} = C_m \frac{du}{dt} + \frac{u}{R_b} + i_c \quad (1)$$

$$\tau_d \frac{di_c}{dt} = \frac{i_{c0}}{1+e^{-(u-V_T)/V_m}} - i_c \quad (2)$$

The model has three independent variables: I_{tot} , u are the external current and voltage, and i_c is an internal current. Eq. (1) describes the three components of I_{tot} : a capacitive charging of the interfaces with capacitance C_m , a small ohmic current of constant resistance R_b , and the slow internal current i_c described by Eq. (2). As described before,³² Eq. (2) represents a diffusion or migration time of ions that introduces a delay of i_c with respect to the external perturbation, by the characteristic time constant τ_d . In the steady state the slow current takes the value

$$i_c = i_{c0} f_{ss}(u) \quad (3)$$

according to the function

$$f_{ss} = \frac{1}{1+e^{-(u-V_T)/V_m}} \quad (4)$$

that varies from 0 at low voltage to 1 at high voltage, with the redox potential V_T and an ideality factor V_m with dimension of voltage. Consequently the slow current varies from 0 to a saturation value i_{c0} depending on the applied voltage. Specific physical mechanisms behind the function f_{ss} are the filamentary conductive pathway²⁰ or the decrease of a surface barrier between the perovskite layer and the contacts.^{36,37} However filamentary systems usually show an abrupt transition to the high conduction state and the above model is adapted to those systems that show a gradual transition.

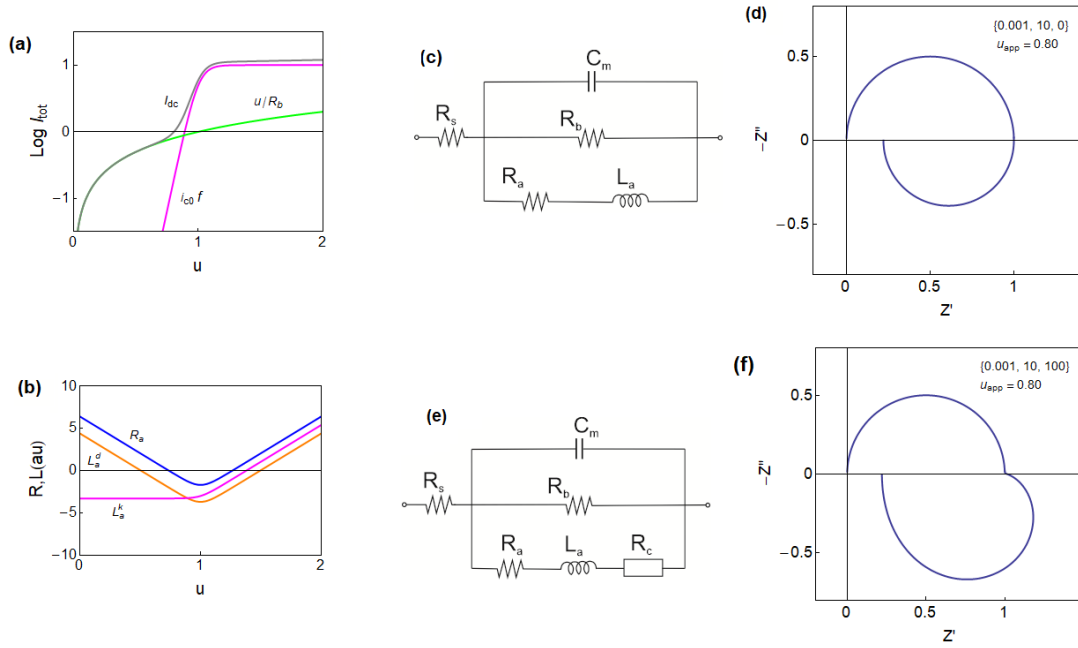


Fig. 1. (a) Logarithmic current-voltage curve for the model memristor, showing the two component currents and the total equilibrium dc current (gray line). (b) Impedance parameters. (c) Equivalent circuit of Eqs. (1, 2) and the impedance spectrum in the indicated conditions (d). (e) Equivalent circuit of Eqs. (1, 10, 11) and impedance spectrum (f). Parameters: $R_b = 1$; $i_{c0} = 10$, $V_T = 1$, $V_m = 0.05$, $[\tau_m, \tau_d, \tau_k]$.

Combining (1), and (3) we find the steady state current-voltage equation is

$$I_{\text{app}} = \frac{u_{\text{app}}}{R_b} + \frac{1}{1 + e^{-(u_{\text{app}} - V_T)/V_m}} i_{c0} \quad (5)$$

The total current of the memristor (grey line) and the component currents are shown in Fig. 1a.

By linearization of Eqs. (1-3) at a steady-state point it can be obtained the impedance spectroscopy response function in terms of the variable $s = i\omega$, where ω is the angular frequency of the small perturbation. The impedance model is

$$Z(s) = \left[C_m s + R_b^{-1} + \frac{1}{R_a + L_a^d s} \right]^{-1} \quad (6)$$

$$R_a^{-1} = \frac{di_c}{du} = \frac{i_{c0}}{V_m} f_{ss} (1 - f_{ss}) \quad (7)$$

$$L_a^d = \tau_d R_a \quad (8)$$

The model of Eq. (6) is the recently described impedance of a chemical inductor.¹⁷ It is characteristically observed in halide perovskite devices in the high voltage domain.^{38,39} The equivalent circuit is shown in Fig. 1c, impedance parameters are shown in Fig. 1b, and the characteristic spectrum with the inductive component in the fourth quadrant is shown in Fig. 1d. The interpretation of EC elements of Fig. 1c is as follows. C_m is a

capacitance element as already mentioned. In the halide perovskites there are two dominant capacitances.^{32,39,40} The geometric capacitance C_g stands for dielectric relaxation at high frequency and it is independent of the voltage. On the other hand a low frequency capacitance C_1 is related to ionic polarization of the interface. C_1 is voltage and light-dependent and takes very large values. The elements resistance R_a and inductor L_a^d are the components of the chemical inductor branch in the equivalent circuit. These elements are formed by the delay equation,¹⁷ in our case Eq. (2), that is interpreted as an electronic current that depends on ionic displacement.^{32,41}

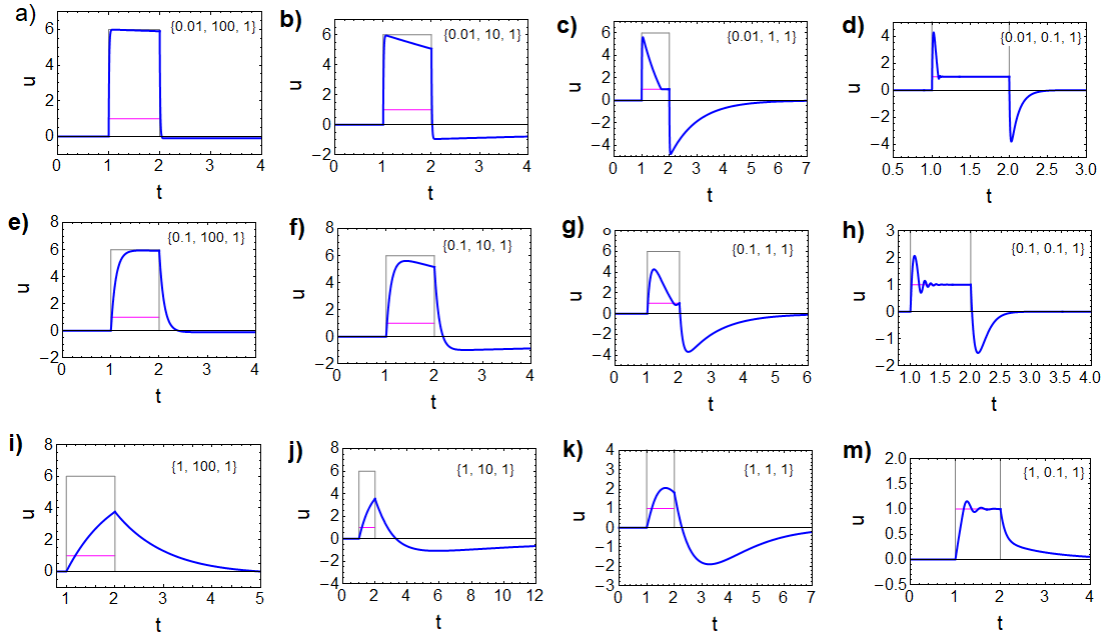


Fig. 2. Time transient response to current steps of value $I_{app}(u_{app})$ and duration Δt . The grey line is the current pulse indicated by the voltage $R_b I_{app}$. The magenta line is the pulse voltage at equilibrium $u_{app} = 1$. $[\tau_m, \tau_d, \Delta t]$ as indicated, and $R_b = 1$; $i_{c0} = 10$ all cases.

Time transient response of the two-dimensional model

We analyze the time transient response of the model to a square perturbation, that was not studied in the previous publication.³² This analysis is particularly important for the formation of analog response of artificial neurons and synapses. In the experiments, the sample is pulsed repetitively and the changing response is recorded.^{30,34} The output in response to a pulsed perturbation can be obtained by the solution of Eqs. (1-2). The transient response is controlled by two main time constants in the model: $\tau_m = R_b C_m$, τ_d , and by the pulse duration time Δt , so that different responses to a step perturbation are expected, according to their combinations. A representative set of responses to a square

current perturbation I_{app} with $R_s = 0$ is shown in Fig. 2. The different behaviours can be interpreted in terms of the model EC of the chemical inductor of Fig. 1c. Note, however, that the circuit is strictly valid only for a small perturbation. When the large external perturbation is applied, the circuit elements are not constant, but undergo the variations shown in Fig. 1b. In a detailed analysis the response times include the total resistances of the network, instead of the simplified time constants τ_m, τ_d . The calculation tool to explore all the possibilities is provided in Supporting Information.

In Fig. 2 the capacitor C_m is charged within the time constant τ_m producing a voltage $I_{app}R_b$ (indicated by the gray line). The inductor line responds with the time constant $\tau_d = L_a^d/R_a$. The magenta line is the final equilibrium voltage of the activated state, with the dc resistance

$$R_{dc} = (R_b^{-1} + R_a^{-1})^{-1} \quad (9)$$

In Fig 2a we start with a very short τ_m charging time. The current rises instantaneously to the grey level, and since the inductor is large, the magenta line will be achieved only at extremely long times. For smaller inductor values in Fig. 2d-c we observe the inductive negative spike reaching the dc voltage value of the square pulse, and a negative discharge characteristics when the pulse is switched off. In Fig. 2e we combine a longer charging time and a very large inductor. The response is the typical RC charging process to the grey reference and subsequent discharge. For smaller inductor values in Fig. 2f-g the decay of initial current peak reaches the stationary line. For the very small inductor value in Fig. 2h the system displays overdamped oscillations.

By using a larger τ_m (or a shorter pulse time), in Fig. 2i the signal is not allowed to reach the grey saturation value. Then for smaller inductor values, Fig. 2f, we have a raising feature in charge but a negative spike in discharge due to the chemical inductor. This pattern reproduces closely the natural shape of the action potential in biological neurons. This action potential is associated to a single square perturbation and not to self-sustained oscillations; we note that the oscillations are damped and vanish in Fig. 2h-m. The general conditions for obtaining stationary oscillations in a two dimensional dynamical model have been reviewed,¹⁶ and it has been concluded that an internal negative resistance sector in dc conditions is necessary to destabilize the system and produce a Hopf bifurcation, as in the FitzHugh-Nagumo model.¹² Instabilities and bifurcation can happen in two-dimensional models in the presence of time-delayed coupling,⁴² which is not considered here. In consequence, the model of Eqs. (1-2) cannot produce a bifurcation and limit cycle oscillations, as it lacks the negative resistance feature.

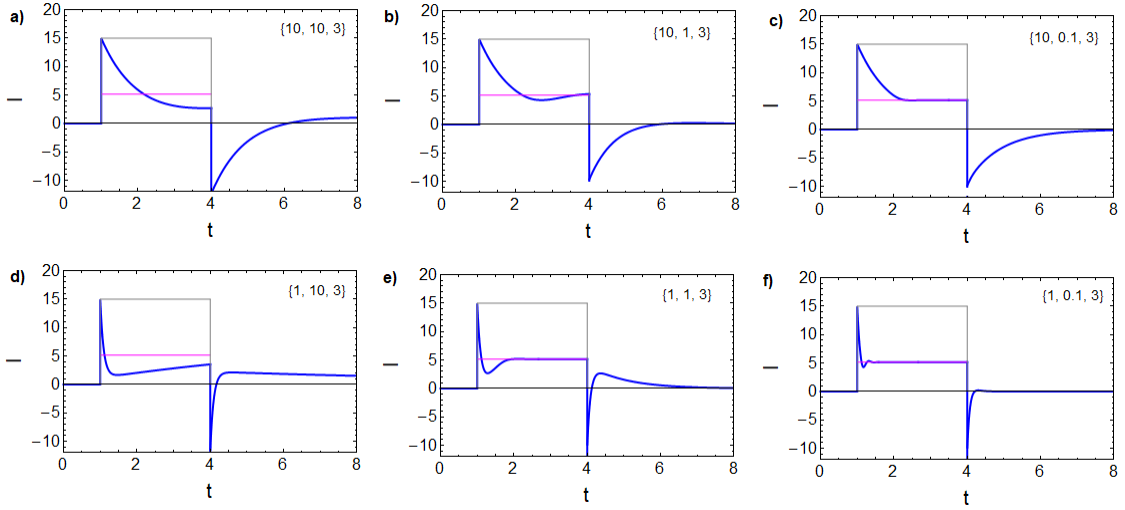


Fig. 3. Time transient response to voltage step of value $V_{app} = 1.5$ V and duration Δt . The grey line is the initial value of the current when the applied voltage lies at the series resistance, V_{app}/R_s and the magenta line is the pulse current at equilibrium $I_{app} = I_{tot}(V_{app})$. $[\tau_m, \tau_d, \Delta t]$ as indicated, $R_s = 0.1$; $R_b = 1$; $i_{c0} = 10$ all cases.

For the calculation of the transient current to a step of the external voltage V_{app} we add the voltage drop across the series resistance according to

$$V_{app} = R_s I_{tot} + u \quad (10)$$

The results are shown in Fig. 3.

The three-dimensional model

We proceed to a more general model describe before.³² In this model we use again the Eq. (1) but we introduce two slow variables, i_c and f , described by the following equations:

$$\tau_d \frac{di_c}{dt} = i_{c0} f - i_c \quad (11)$$

$$\tau_k \frac{df}{dt} = (1 - f) - e^{-\frac{u-V_T}{v_m}} f \quad (12)$$

Eq. (12) describes the voltage-controlled activation of the high conduction configuration. τ_k is the characteristic formation time of the high conduction state. The variable f is an occupation function ($0 \leq f \leq 1$) that describes the onset of the memristor activated state. Similarly to the ion channel behaviour in neurons,² the variable f indicates the state of the mechanism that establishes the high conductivity state in the memristor. As commented in Eq. (2) the parameter τ_d in Eq. (11) indicates the diffusion time necessary to establish the configuration of high f that produces the large electronic current i_{c0} .

If we consider the steady state situation we obtain again Eqs. (3) and (4) and the current

voltage is given by Eq. (5). If we assume that formation time τ_k is short, then Eq. (12) leads to quasi equilibrium condition $f \approx f_{ss}$ and the model becomes the two-dimensional set Eqs. (1-2) that we analyzed before. In the three dimensional model the transient response is controlled by three main time constants: $\tau_m = R_b C_m, \tau_d, \tau_k$, and by the pulse time duration.

The impedance of the three dimensional model has the form³²

$$Z(s) = \left[C_m s + R_b^{-1} + \frac{1}{Z_c} \right]^{-1} \quad (13)$$

The Z_c impedance is

$$Z_c(s) = (1 + s\tau_d)(R_a + L_a^k s) \quad (14)$$

These last two equations provide the EC of Fig. 1e. The impedance parameters are defined as before and a new inductor appears due to Eq. (12)

$$L_a^k = f\tau_k R_a \quad (15)$$

We can write Eq. (15) as

$$Z_c(\omega) = R_a + i\omega L_a^k + i\omega L_a^d + R_c(\omega) \quad (16)$$

where

$$R_c(\omega) = -\frac{L_a^k L_a^d}{R_a} \omega^2 \quad (17)$$

The impedance spectra have been fully described³² and a representative example showing a RC arc at high frequency and a distorted inductive arc at low frequency is shown in Fig. 1f. This type of spectra has been observed experimentally in halide perovskite memristors,³² giving strong support to the relevance of the model.

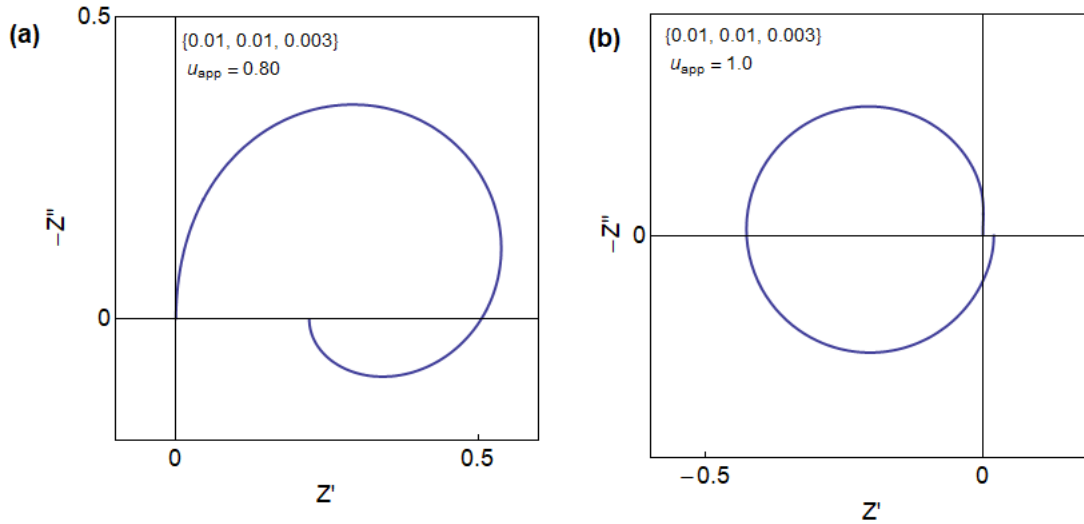


Fig. 4. Impedance spectra of the model memristor of Eqs. (1, 10, 11) in the indicated conditions. Parameters: $R_b = 1$; $i_{c0} = 10$, $V_T = 1$, $V_m = 0.05$, $[\tau_m, \tau_d, \tau_k]$.

Bifurcation and self-sustained oscillations

In Fig. 4 we show the impedance spectra of the general three-dimensional model, Eqs. (1, 11-12), for a different set of kinetic parameters in comparison to Fig. 1f. The Fig. 4a is the normal form of the inductive spectrum of a chemical inductor shown in Fig. 1d.¹⁷ But Fig. 4b presents a *negative resistance* at a finite frequency. This pattern occurs in a narrow voltage range around the transition region of the memristor, as discussed later. The spectrum of Fig. 4b is the characteristic mark of a Hopf bifurcation that causes self-sustained oscillations in electrochemical systems and neurons, in galvanostatic conditions.^{12,16,43}

Our model, however, does not contain a negative resistance component, as already commented, since the $I - u$ curve in Fig. 1a is formed by strictly positive dc resistances. In the present system, the negative resistance is caused by the coupling of two inductive features that produce the element $R_c(\omega)$ of Eq. (17). It is a *dynamical instability* that exists at nonzero frequency and disappears in dc conditions.

Since the reported general analysis of bifurcation by IS¹⁶ is restricted to two-dimensional systems, we apply the normal mode method¹⁰ to the current system. From the linearized equations of (1, 11-12) we find the Jacobian

$$\begin{pmatrix} -\frac{1}{\tau_m} & -\frac{1}{C_m} & 0 \\ 0 & -\frac{1}{\tau_d} & \frac{i_{c0}}{\tau_d} \\ \frac{1-f}{\tau_k V_m} & 0 & -\frac{1}{f\tau_k} \end{pmatrix} \quad (\text{SI18})$$

The characteristic equation for the eigenvalues λ has the form

$$\lambda^3 + c_2\lambda^2 + c_1\lambda + c_0 = 0 \quad (19)$$

where the coefficients are given by the expressions

$$c_0 = \frac{i_{c0}(1-f)}{\tau_d\tau_k C_m V_m} \quad (20)$$

$$c_1 = \frac{1}{f\tau_d\tau_k} + \frac{1}{f\tau_m\tau_k} + \frac{1}{\tau_d\tau_m} \quad (21)$$

$$c_2 = \frac{1}{\tau_m} + \frac{1}{\tau_d} + \frac{1}{f\tau_k} \quad (22)$$

At the Hopf bifurcation a pair of eigenvalues become purely imaginary.⁴⁴ We insert the form $\lambda = i\varpi$ and we obtain the equations

$$\varpi^2 = c_1 \quad (23)$$

$$\varpi^2 = \frac{c_0}{c_2} \quad (24)$$

Therefore, the Hopf bifurcations occur at the points that satisfy

$$c_1 c_2 = c_0 \quad (25)$$

The different coefficients as functions of voltage are plotted in Fig. 5a. It is observed

that in the crossing of c_0 and $c_1 c_2$ two Hopf bifurcations occur that mark a domain where the system is unstable and can perform limit cycle oscillations. By solving the full three-dimensional system (1, 11-12) in the time domain, the oscillations can be generated as shown in Fig. 5b, c.

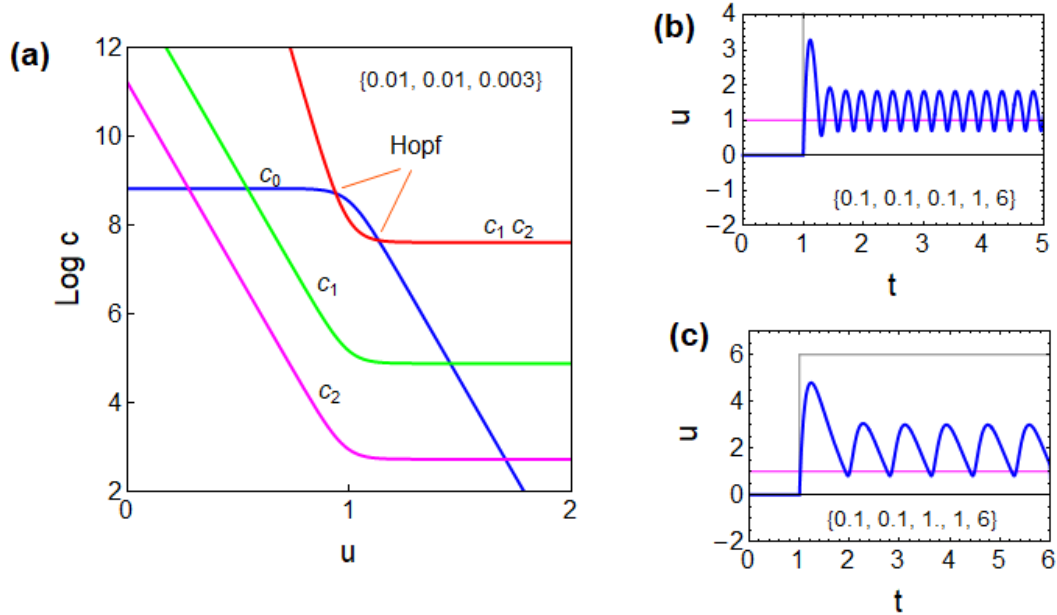


Fig. 5. Model of Eqs. (1, 10-11). (a) Coefficients of the characteristic equation vs. voltage and location of the Hopf bifurcations. $[\tau_m, \tau_d, \tau_k]$ as indicated. (b-c) Time transient response to current steps of value $I_{app}(u_{app})$. The grey line is the current pulse indicated by the voltage $R_b I_{app}$. The magenta line is the voltage at equilibrium u_{app} . $[\tau_m, \tau_d, \tau_k, u_{app}, I_{app}]$ as indicated. $R_b = 1$; $i_{c0} = 10$ all cases.

In conclusion, we analyzed the time domain and impedance response of a three-dimensional memristor dynamical model. In a simplified two-dimensional version, we obtain responses to a pulsed current perturbation in which the main properties of a neuronal action potential can be reproduced with a simple device without internal electronic parts.

In addition, we analyzed the properties of oscillating dynamics. It has been previously established that two-dimensional models require an intrinsic negative resistance, that persists in dc condition, to produce a Hopf bifurcation that moves the system into self-sustained oscillations. Here we find a new property: In the three-dimensional system a Hopf bifurcation occurs without an intrinsic negative resistance. This is because a product of inductors produces a dynamical negative resistance that exists only in transient conditions. So far, such oscillating patterns of the perovskite memristor have not been observed.

Acknowledgment

We thank the financial support by Generalitat Valenciana for a Prometeo grant (PROMETEU/2020/028).

Supporting Information

Mathematica program for calculation of transient responses and impedances.

References

- (1) Stiefel, K. M.; Ermentrout, G. B. Neurons as oscillators, *J. Neurophysiol.* **2016**, *116*, 2950-2960.
- (2) Hodgkin, A. L.; Huxley, A. F. A quantitative description of membrane current and its application to conduction and excitation in nerve, *J Physiol* **1952**, *117*, 500-544.
- (3) Gerstner, W.; Kistler, W. M.; Naud, R.; Paninski, L. *Neuronal Dynamics. From single neurons to networks and models of cognition*; Cambridge University Press, 2014.
- (4) Tuchman, Y.; Mangoma, T. N.; Gkoupidenis, P.; van de Burgt, Y.; John, R. A.; Mathews, N.; Shaheen, S. E.; Daly, R.; Malliaras, G. G.; Salleo, A. Organic neuromorphic devices: Past, present, and future challenges, *MRS Bulletin* **2020**, *45*, 619-630.
- (5) van de Burgt, Y.; Gkoupidenis, P. Organic materials and devices for brain-inspired computing: From artificial implementation to biophysical realism, *MRS Bulletin* **2020**, *45*, 631-640.
- (6) Javad, M.; Hossein, M.; Donati, E.; Yokota, T.; Lee, S.; Indiveri, G.; Someya, T.; Nawrocki, R. A. Organic electronics Axon-Hillock neuromorphic circuit: towards biologically compatible, and physically flexible, integrate-and-fire spiking neural networks, *J. Phys. D: Appl. Phys.* **2021**, *54*, 104004.
- (7) John, R. A.; Tiwari, N.; Patdillah, M. I. B.; Kulkarni, M. R.; Tiwari, N.; Basu, J.; Bose, S. K.; Ankit; Yu, C. J.; Nirmal, A.; Vishwanath, S. K.; Bartolozzi, C.; Basu, A.; Mathews, N. Self healable neuromorphic memtransistor elements for decentralized sensory signal processing in robotics, *Nat. Commun.* **2020**, *11*, 4030.
- (8) Cessac, B.; Viéville, T. On dynamics of integrate-and-fire neural networks with conductance based synapses, *Front. Comput. Neurosci.* **2008**, *2*, 2.
- (9) Harikesh, P. C.; Yang, C.-Y.; Tu, D.; Gerasimov, J. Y.; Dar, A. M.; Armada-Moreira, A.; Massetti, M.; Kroon, R.; Bliman, D.; Olsson, R.; Stavrinidou, E.; Berggren, M.; Fabiano, S. Organic electrochemical neurons and synapses with ion mediated spiking, *Nat. Commun.* **2022**, *13*, 901.
- (10) Scott, S. K. *Chemical Chaos*; Clarendon Press, 1991.
- (11) Izhikevich, E. M. *Dynamical Systems in Neuroscience*; MIT Press, 2007.
- (12) Bisquert, J. A frequency domain analysis of excitability and bifurcations of Fitzhugh-Nagumo neuron model., *J. Phys. Chem. Lett.* **2021**, *12*, 11005–11013.
- (13) Roçşoreanu, C.; Georgescu, A.; Giurgiţeanu, N. *The FitzHugh-Nagumo model: bifurcation and dynamics*; Kluwer Academic Publishers, 2000.
- (14) Kostova, T.; Ravindran, R.; Schonbek, M. Fitzhugh–Nagumo revisited:

types of bifurcations, periodical forcing and stability regions by a Lyapunov functional, *International Journal of Bifurcation and Chaos* **2004**, *14*, 913-925.

(15) Armbruster, D. The (almost) complete dynamics of the Fitzhugh Nagumo equations, *Nonlinear Dynamics* **1997**, *Volume 2*, 89-102.

(16) Bisquert, J. Hopf bifurcations in electrochemical, neuronal, and semiconductor systems analysis by impedance spectroscopy, *Appl. Phys. Rev.* **2022**, *9*, 011318.

(17) Bisquert, J.; Guerrero, A. Chemical Inductor, *J. Am. Chem. Soc.* **2022**, 10.1021/jacs.1022c00777.

(18) Kwak, K. J.; Lee, D. E.; Kim, S. J.; Jang, H. W. Halide Perovskites for Memristive Data Storage and Artificial Synapses, *J. Phys. Chem. Lett.* **2021**, *12*, 8999-9010.

(19) Kang, K.; Hu, W.; Tang, X. Halide Perovskites for Resistive Switching Memory, *J. Phys. Chem. Lett.* **2021**, *12*, 11673-11682.

(20) Fang, Y.; Zhai, S.; Chu, L.; Zhong, J. Advances in Halide Perovskite Memristor from Lead-Based to Lead-Free Materials, *ACS Appl. Mat. Int.* **2021**, *13*, 17141-17157.

(21) Pershin, Y. V.; Di Ventra, M. Memory effects in complex materials and nanoscale systems, *Adv. Phys.* **2011**, *60*, 145-227.

(22) Rahimi Azghadi, M.; Chen, Y.-C.; Eshraghian, J. K.; Chen, J.; Lin, C.-Y.; Amirsoleimani, A.; Mehonic, A.; Kenyon, A. J.; Fowler, B.; Lee, J. C.; Chang, Y.-F. Complementary Metal-Oxide Semiconductor and Memristive Hardware for Neuromorphic Computing, *Advanced Intelligent Systems* **2020**, *2*, 1900189.

(23) Gogoi, H. J.; Bajpai, K.; Mallajosyula, A. T.; Solanki, A. Advances in Flexible Memristors with Hybrid Perovskites, *J. Phys. Chem. Lett.* **2021**, *12*, 8798-8825.

(24) Bou, A.; Bisquert, J. Impedance spectroscopy dynamics of biological neural elements: from memristors to neurons and synapses, *J. Phys. Chem. B* **2021**, *125* 9934–9949.

(25) Mehonic, A.; Kenyon, A. J. Emulating the Electrical Activity of the Neuron Using a Silicon Oxide RRAM Cell, *Frontiers in Neuroscience* **2016**, *10*.

(26) Gong, J.; Wei, H.; Ni, Y.; Zhang, S.; Du, Y.; Xu, W. Methylammonium halide-doped perovskite artificial synapse for light-assisted environmental perception and learning, *Materials Today Physics* **2021**, *21*, 100540.

(27) Christensen, D. V.; Dittmann, R.; Linares-Barranco, B.; Sebastian, A.; Le Gallo, M. 2022 roadmap on neuromorphic computing and engineering, *Neuromorphic Computing and Engineering* **2022**, DOI: 10.1088/2634-4386/ac1084a1083.

(28) Choi, J.; Han, J. S.; Hong, K.; Kim, S. Y.; Jang, H. W. Organic–Inorganic

Hybrid Halide Perovskites for Memories, Transistors, and Artificial Synapses, *Adv. Mater.* **2018**, *30*, 1704002.

(29) Xu, W.; Cho, H.; Kim, Y.-H.; Kim, Y.-T.; Wolf, C.; Park, C.-G.; Lee, T.-W. Organometal Halide Perovskite Artificial Synapses, *Adv. Mater.* **2016**, *28*, 5916-5922.

(30) Yang, J.-Q.; Wang, R.; Wang, Z.-P.; Ma, Q.-Y.; Mao, J.-Y.; Ren, Y.; Yang, X.; Zhou, Y.; Han, S.-T. Leaky integrate-and-fire neurons based on perovskite memristor for spiking neural networks, *Nano Energy* **2020**, *74*, 104828.

(31) Gong, J.; Yu, H.; Zhou, X.; Wei, H.; Ma, M.; Han, H.; Zhang, S.; Ni, Y.; Li, Y.; Xu, W. Lateral Artificial Synapses on Hybrid Perovskite Platelets with Modulated Neuroplasticity, *Adv. Func. Mater.* **2020**, *30*, 2005413.

(32) Berruet, M.; Pérez-Martínez, J. C.; Romero, B.; Gonzales, C.; Al-Mayouf, A. M.; Guerrero, A.; Bisquert, J. Physical model for the current-voltage hysteresis and impedance of halide perovskite memristors, *ACS Energy Lett.* **2022**, *7*, 1214–1222.

(33) Gumyusenge, A.; Melianas, A.; Keene, S. T.; Salleo, A. Materials Strategies for Organic Neuromorphic Devices, **2021**, *51*, 47-71.

(34) John, R. A.; Yantara, N.; Ng, S. E.; Patdillah, M. I. B.; Kulkarni, M. R.; Jamaludin, N. F.; Basu, J.; Ankit; Mhaisalkar, S. G.; Basu, A.; Mathews, N. Diffusive and Drift Halide Perovskite Memristive Barristors as Nociceptive and Synaptic Emulators for Neuromorphic Computing, *Adv. Mater.* **2021**, *33*, 2007851.

(35) John, R. A.; Yantara, N.; Ng, Y. F.; Narasimman, G.; Mosconi, E.; Meggiolaro, D.; Kulkarni, M. R.; Gopalakrishnan, P. K.; Nguyen, C. A.; De Angelis, F.; Mhaisalkar, S. G.; Basu, A.; Mathews, N. Ionotronic Halide Perovskite Drift-Diffusive Synapses for Low-Power Neuromorphic Computation, *Adv. Mater.* **2018**, *30*, 1805454.

(36) Solanki, A.; Guerrero, A.; Zhang, Q.; Bisquert, J.; Sum, T. C. Interfacial Mechanism for Efficient Resistive Switching in Ruddlesden-Popper Perovskites for Non-Volatile Memories, *J. Phys. Chem. Lett.* **2020**, *11*, 463-470.

(37) Yang, J. J.; Strukov, D. B.; Stewart, D. R. Memristive devices for computing, *Nature Nanotechnology* **2013**, *8*, 13-24.

(38) Bisquert, J.; Guerrero, A.; Gonzales, C. Theory of Hysteresis in Halide Perovskites by Integration of the Equivalent Circuit, *ACS Phys. Chem Au* **2021**, *1*, 25-44.

(39) Guerrero, A.; Bisquert, J.; Garcia-Belmonte, G. Impedance spectroscopy of metal halide perovskite solar cells from the perspective of equivalent circuits, *Chemical Reviews* **2021**, *121*, 14430–14484.

(40) Taukeer Khan, M.; Khan, F.; Al-Ahmed, A.; Ahmad, S.; Al-Sulaiman, F. Evaluating the Capacitive Response in Metal Halide Perovskite Solar Cells, *The Chemical Record* **2022**, *n/a*, e202100330.

(41) Pockett, A.; Carnie, M. J. Ionic Influences on Recombination in Perovskite

Solar Cells, *ACS Energy Lett.* **2017**, *2*, 1683-1689.

(42) Bisquert, J. The impedance of spiking neurons coupled by time-delayed interaction, *physica status solidi (a)* **2022**, <https://doi.org/10.1002/pssa.202200064>.

(43) T. M. Koper, M. Non-linear phenomena in electrochemical systems, *Journal of the Chemical Society, Faraday Transactions* **1998**, *94*, 1369-1378.

(44) Guckenheimer, J.; Myers, M. Computing Hopf Bifurcations. II: Three Examples From Neurophysiology, *SIAM Journal on Scientific Computing* **1996**, *17*, 1275-1301.